Effect of halogen on the luminescence properties of two-dimensional double-perovskite $(C_6H_{16}N_2)_2AgBiX_8{\cdot}H_2O$ ($X = Cl,\ Br$ and I) with the Dion-Jacobson structure

Jun Luo,[1] Biao Liu,[2] Jun-Liang Yang,[2] and Meng-Qiu Cai[1,3,*]

[1] *Hunan Provincial Key Laboratory of High-Energy Scale Physics and Applications, School of Physics and Electronics, Hunan University, Changsha 410082, China*

[2] *Hunan Key Laboratory for Super-microstructure and Ultrafast Process, School of Physics and Electronics, Central South University, Changsha 410083, Hunan, China*

[3] *Greater Bay Area Institute for Innovation, Hunan University, Guangzhou 511300, China*

(Received 16 April 2024; revised 11 June 2024; accepted 3 July 2024; published 25 July 2024)

Two-dimensional (2D) metal halide perovskites have garnered significant attention in the field of light-emitting diodes due to their high photoluminescence quantum yield and tunability. In comparison with the widely studied 2D Ruddlesden-Popper (RP) perovskites, the 2D Dion-Jacobson (DJ) double perovskites, which offer higher stability and nontoxicity, have received relatively less attention. In addition, the regulatory effects of halogens on the luminescence mechanisms and performance of 2D DJ double perovskites remain unknown. Utilizing density functional theory, the stability and luminescence properties of 2D DJ double-perovskite $(C_6H_{16}N_2)_2AgBiX_8{\cdot}H_2O$ ($X = Cl,\ Br,\ I$) are effectively modulated through halogen substitution. The findings indicate that the dissociation energy incrementally increases as the halogen changes from I to Br to Cl, suggesting that the incorporation of lighter halogens enhances structural stability. The minimal self-trapping formation energy (i.e., 0.08 eV) of $(C_6H_{16}N_2)_2AgBiI_8{\cdot}H_2O$ facilitates easy detrapment of self-trapped excitons, leading to a tendency toward free exciton luminescence. The self-trapping formation energies of $(C_6H_{16}N_2)_2AgBiBr_8{\cdot}H_2O$ and $(C_6H_{16}N_2)_2AgBiCl_8{\cdot}H_2O$ are 0.77 eV and 0.96 eV, respectively, indicating substantial self-trapping depths; thus, favoring self-trapped exciton luminescence. In addition, the transition dipole moments of $(C_6H_{16}N_2)_2AgBiBr_8{\cdot}H_2O$ and $(C_6H_{16}N_2)_2AgBiCl_8{\cdot}H_2O$ are substantially higher than those of $(C_6H_{16}N_2)_2AgBiI_8{\cdot}H_2O$, suggesting that substituting I with Cl and Br enhances the luminous efficiency of 2D DJ double-perovskite $(C_6H_{16}N_2)_2AgBiX_8{\cdot}H_2O$ ($X = Cl,\ Br,\ I$). These results indicate that halogen substitution can not only affect the stability of 2D DJ perovskites but also modulate their luminescent properties. Our research provides theoretical insights for the experimental design of superior luminescent materials.

DOI: 10.1103/PhysRevApplied.22.014064

I. INTRODUCTION

Due to their structural diversity, luminescence tunability, and high photoluminescence quantum yield (PLQY), two-dimensional (2D) perovskites hold significant potential in the field of luminescence [1–6]. 2D halide perovskites can be divided into two main types, i.e., Dion-Jacobson (DJ) and Ruddlesden-Popper (RP) structures, according to the charge on the interlayer cations [7,8]. In RP-phase perovskites, the amine groups of the long-chain organic cations form hydrogen bonds with the halogens of the metal halide octahedra at the inorganic layer boundary. The adjacent organic layers are linked by van der Waals interactions between the organic cations, with the inorganic layer displaying (1/2, 1/2)-in-plane displacement along the *ab*-plane in each unit cell. In DJ-phase perovskites, the long chain of organic amines is a diamine compound, with amines at both ends forming hydrogen bonds with the halogens of the two adjacent boundary metal halide octahedra, similar to the RP phase. The absence of van der Waals interactions between adjacent organic layers results in a complete overlap of adjacent inorganic layers without any in-plane migration along the *ab*-plane. Therefore, compared with RP-phase perovskites, the lack of van der Waals interactions between adjacent organic layers in DJ-phase perovskites may be one of the key reasons for the stability differences between RP-phase and DJ-phase perovskites. In 2018, Mao *et al.* [8] first synthesized 2D DJ-phase organic-inorganic hybrid perovskite, utilizing 3AMP (3-ammethylpiperidine) and 4AMP (4-ammethylpiperidine) to prepare $(A')(MA)_{n-1}Pb_n\ I_{3n+1}$ ($A' = 3AMP$ or 4AMP,

*Contact author: mqcai@hnu.edu.cn

$n = 1$–4). These perovskites demonstrated excellent air stability. Shang *et al*. [1], while exploring high-stability 2D perovskite light-emitting diodes, found that the half-life of light-emitting diodes based on DJ structures exceeds 100 h, nearly two orders of magnitude longer than the half-life of light-emitting diodes based on 2D perovskites involving RP structures. These studies indicate that DJ structures indeed possess advantages in stability compared with RP structures.

In the original structure of lead halide perovskites, a double-perovskite structure is formed by substituting a pair of lead ions with a monovalent cation and a trivalent cation. Double perovskites are considered effective alternatives to lead halide perovskites since they are free of toxic elements and retain an octahedral structure similar to perovskites, which has garnered significant attention in recent years. Currently, double-perovskite materials have achieved numerous successes in the field of light-emitting diodes [9–11]. For instance, Tang's team achieved an exceptionally high photoluminescence quantum yield (PLQY) of 86% for warm white light emission in three-dimensional double-perovskite $Cs_2(Ag_{0.60}Na_{0.40})InCl_6$ [12]. Manna *et al*. enhanced the PLQY of three-dimensional double-perovskite $Cs_2AgInCl_6$ nanocrystals by an order of magnitude through Mn^{2+} doping, which clearly demonstrates the tunability of double-perovskite luminescence properties [13]. However, most attention has focused on three-dimensional double perovskites, with relatively little interest given to 2D double perovskites. Three-dimensional metal halide perovskites typically exhibit narrowband luminescence from free exciton recombination, whereas one- and zero-dimensional metal halide perovskites generally display broadband luminescence from self-trapped exciton recombination. However, the luminescence characteristics of 2D perovskites are diverse, with some exhibiting free exciton recombination luminescence and others displaying self-trapped exciton recombination luminescence. We compiled the luminescence characteristics of recently studied 2D perovskites, which are presented in the Supplemental Material (see Table S1) [61]. It was observed that most 2D Cl- and Br-based perovskites exhibit broadband emission with large Stokes shifts, whereas 2D I-based perovskites display narrowband emission with small Stokes shifts. Therefore, halogen substitution is anticipated to alter the luminescence mechanisms of 2D perovskites and regulate their properties.

Recently, Le *et al*. successfully synthesized 2D DJ double-perovskite $(C_6H_{16}N_2)_2AgBiI_8{\cdot}H_2O$, performing thermogravimetric analysis and observing no significant mass loss until the temperature reached 300 °C, indicating stability under normal conditions [14]. Furthermore, they discovered that 2D DJ double-perovskite $(C_6H_{16}N_2)_2AgBiI_8{\cdot}H_2O$ exhibited significant photoconductivity under xenon lamp irradiation, indicating its potential for application as an optoelectronic material. This study utilizes $(C_6H_{16}N_2)_2AgBiI_8{\cdot}H_2O$ as a prototype to investigate the effects of halogen substitution on the luminescence properties and stability of 2D DJ double-perovskite $(C_6H_{16}N_2)_2AgBiX_8{\cdot}H_2O$ ($X = $ Cl, Br, I).

II. COMPUTATIONAL METHODS

A. Density functional theory calculations

Density functional theory (DFT) calculations were performed based on the Vienna *ab initio* simulation package (VASP) [15,16]. The Perdew-Burke-Ernzerhof (PBE) method within the generalized gradient approximation and the projection augmented wave method are used to describe the interaction and exchange-correlation effects between valence electrons and ion nuclei [17–20]. The energy cutoff of the plane-wave cutoff was set at 400 eV in all the calculations [21–23]. A $4 \times 4 \times 2$ k-mesh sampling Monkhorst–Park scheme was used in the full optimization for 2D DJ double-perovskite $(C_6H_{16}N_2)_2AgBiX_8{\cdot}H_2O$ ($X = $ Cl, Br, and I) until the force tolerance of each atom was less than 0.03 eV/Å [24]. The DFT-D3 function was used to account for weak van der Waals (vdW) Interaction.

B. Dissociation energy calculations

The molecular dissociation energy refers to the energy required for organic groups to detach from the lattice. The formula for calculating the dissociation energy of molecules (organic groups) is as follows:

$$E_{\text{dissociation}} = E_{\text{remain}} + E_{\text{molecule}} - E_{\text{supercell}}, \tag{1}$$

where $E_{\text{dissociation}}$ represents the molecule dissociation energy, E_{remain} signifies the total energy of the remaining structure after the dissociation of the molecule, E_{molecule} is the total energy of the dissociated molecule, and $E_{\text{supercell}}$ represents the total energy of the perfect supercell [1]. The dissociation energy calculation used a $2 \times 1 \times 1$ supercell.

C. Effective mass

The effective mass m^* is an important parameter to describe the motion characteristics of carriers in semiconductors. It can be calculated by fitting the energy-momentum relationship in the band structure. To fit the energy-momentum relationship near the conduction band minimum (or valence band maximum), we use the following parabolic equation:

$$E(k) = \frac{\hbar^2 k^2}{2m^*}, \tag{2}$$

where E is the energy, k is the wave vector, and $\hbar$ is the reduced Planck constant. The coefficients obtained from the parabolic fitting can be used to calculate the effective mass m^* [25].

D. Exciton binding energy

The exciton binding energy E_b is the Coulomb energy that needs to be overcome for electrons and holes to form excitons. For different quantum states of excitons, the binding energy can be estimated using an empirical formula that includes the quantum number n. Based on the Wannier exciton model, the exciton binding energy is given by [26]

$$E_b = \frac{m_r^* e^4}{2(4\pi\varepsilon_0\varepsilon_\infty)^2\hbar^2 n^2}. \quad (3)$$

Here, m_r^* is the reduced mass of electrons and holes, defined as $(1/m_r^* = 1/m_e^* + 1/m_h^*)$; is the static dielectric constants contributed from an electron [27], which can be evaluated by usε_∞ing density functional perturbation theory. Moreover, e is the electron charge. ε_0 is the vacuum permittivity, ε_∞ is the relative permittivity of the material, and n is the principal quantum number of the exciton state. In our calculation, the exciton energy level n equals one, which signifies the exciton ground state energy.

E. Calculation of the excited-state structure

All the excited-state structures in this paper are calculated using the delta self-consistent field method. The specific approach is to first move an electron from the highest occupied state to the lowest unoccupied state. Next, the occupation is kept unchanged, the structure is relaxed, and the stable excited-state structure is obtained [28].

III. RESULTS AND DISCUSSION

Figure 1 presents a schematic crystal structure of 2D DJ double-perovskite $(C_6H_{16}N_2)_2AgBiX_8{\cdot}H_2O$ (X = Cl, Br, I), which belongs to the triclinic crystal system. As depicted in the figure, the inorganic layer comprises $[BiX_6]^{4-}$ and $[AgX_6]^{4-}$ octahedra (X = Cl, Br, I) interconnected by halogen atoms. The irregular plate structure of 1,4-cyclohexanediamine increases the contact area between molecules, thereby enhancing intermolecular interaction forces and preventing relative sliding between organic molecules, resulting in a highly stable material structure. The 2D DJ double perovskites $(C_6H_{16}N_2)_2AgBiX_8{\cdot}H_2O$ (X = Cl, Br, I) adopt a typical 2D layered DJ perovskite framework with short interlayer distances. The interlayer distance for $(C_6H_{16}N_2)_2AgBiI_8{\cdot}H_2O$ is 3.869 Å [see Fig. 1(a)], for $(C_6H_{16}N_2)_2AgBiBr_8{\cdot}H_2O$ it is 4.015 Å [see Fig. S7(a) in the Supplemental Material], and for $(C_6H_{16}N_2)_2AgBiCl_8{\cdot}H_2O$ it is 4.223 Å [see Fig. S7(b) within the Supplemental Material [61]]. The interlayer distance of $(C_6H_{16}N_2)_2AgBiX_8{\cdot}H_2O$ (X = Cl, Br, I) is comparable to that of 2D DJ lead perovskite [(4AMPY)$(MA)_6Pb_2I_7$, 4.006 Å] [25] and shorter than that of 2D RP double perovskites [$(BA)_4AgBiBr_8$, 7.65673 Å, and $(BA)_2CsAgBiBr_7$, 8.271183 Å] [29].

Due to their soft structure, the organic groups in 2D organic-inorganic hybrid perovskites can move under external fields, leading to structural transformations of the perovskite [30–32]. Consequently, many high-efficiency organic-inorganic hybrid perovskite luminescent materials can only sustain peak efficiency for a limited duration [33]. The dissociation energy reflects the difficulty of organic groups detaching from the perovskite crystal lattice. Therefore, by comparing dissociation energy values, we can evaluate the stability of organic-inorganic hybrid perovskite structures. Based on this fact, we compared the stability of 2D RP double-perovskite $(BA)_4BiAgBr_8$ with 2D DJ double-perovskite $(C_6H_{16}N_2)_2AgBiX_8{\cdot}H_2O$

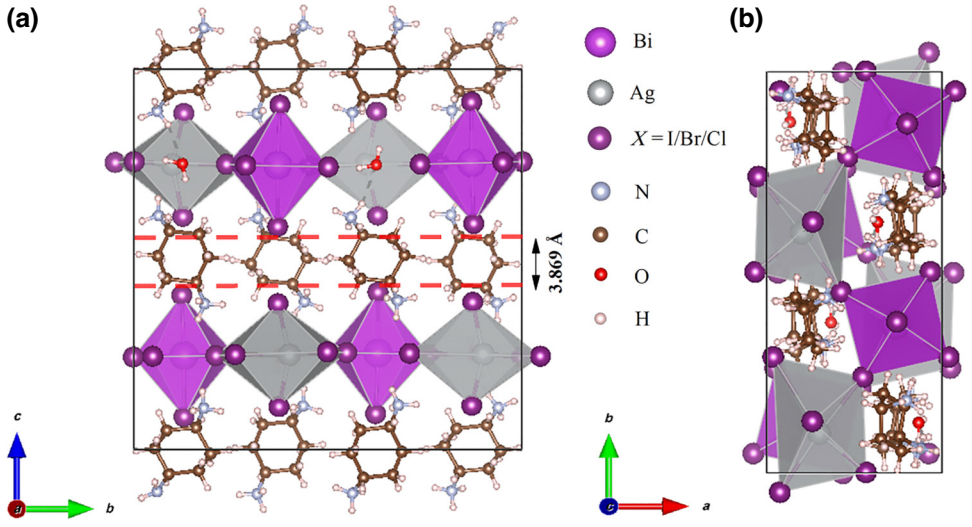

FIG. 1. (a) Crystal structures of 2D DJ double-perovskite $(C_6H_{16}N_2)_2AgBiX_8{\cdot}H_2O$ (X = Cl, Br, I). The red dotted line indicates the layer spacing. (b) Top view of 2D DJ double-perovskite $(C_6H_{16}N_2)_2AgBiX_8{\cdot}H_2O$ (X = Cl, Br, I).

(X = Cl, Br, I). Both perovskites share the same octahedral composition, comprising silver and bismuth octahedra, making them ideal for comparing the stability differences between 2D RP and 2D DJ double perovskites. The results indicate that the dissociation energy of 2D DJ double-perovskite $(C_6H_{16}N_2)_2AgBiX_8{\cdot}H_2O$ (X = Cl, Br, I) exceeds 10 eV, significantly higher than that of 2D RP double-perovskite $(BA)_4BiAgBr_8$, which is 5.43 eV. This is attributed to DJ perovskites having shorter interlayer distances compared with RP perovskites, resulting in tighter binding of inorganic units to organic units, making it more difficult for organic groups to dissociate from the structure, thereby exhibiting higher stability.

It is well-known that iodide perovskites are the most challenging to synthesize due to their lower stability compared with chloride and bromide perovskites. Therefore, we investigated the effects of different halogens on the stability of 2D DJ double-perovskite $(C_6H_{16}N_2)_2AgBiX_8{\cdot}H_2O$ (X = Cl, Br, I). The results demonstrate that the dissociation energy of $(C_6H_{16}N_2)_2AgBiCl_8{\cdot}H_2O$ is higher than that of $(C_6H_{16}N_2)_2AgBiBr_8{\cdot}H_2O$ and $(C_6H_{16}N_2)_2AgBiI_8{\cdot}H_2O$, confirming from a molecular dissociation perspective that substituting I with Cl or Br enhances structural stability. The role of water molecules in the perovskite structure has been studied extensively. Existing studies suggest that water can be both beneficial and detrimental to perovskites [34–38]. In this study, we examine the impact of water molecules on the stability of 2D DJ double-perovskite $(C_6H_{16}N_2)_2AgBiX_8{\cdot}H_2O$ (X = Cl, Br, I) exclusively from a stability perspective. In 2D DJ double perovskites, water molecules link two organic groups through hydrogen bonds, causing these two organic groups to function as a single unit. This structure potentially increases the stability of the organic groups and makes them harder to dissociate, thereby enhancing the overall stability of the crystal structure.

To validate this hypothesis, we first relaxed 2D DJ double-perovskite $(C_6H_{16}N_2)_2AgBiX_8$ until force convergence was achieved. Subsequently, we calculated their dissociation energies. The results indicate that regardless of whether X is Cl, Br, or I, the dissociation energy of $(C_6H_{16}N_2)_2AgBiX_8$ (X = Cl, Br, I) is lower than that of $(C_6H_{16}N_2)_2AgBiX_8{\cdot}H_2O$ (X = Cl, Br, I), confirming that water molecules indeed contribute to stabilizing the structure. In addition, the dissociation energy of $(C_6H_{16}N_2)_2AgBiCl_8$ is greater than that of $(C_6H_{16}N_2)_2AgBiBr_8$, which is greater than that of $(C_6H_{16}N_2)_2AgBiI_8$, demonstrating that water molecules do not interfere with the regulation of structural stability by halogens. All the calculated dissociation energy results are presented in Table I.

The band structure of 2D DJ double-perovskite $(C_6H_{16}N_2)_2AgBiX_8{\cdot}H_2O$ (X = Cl, Br, I) was computed using the PBE, PBE + SOC, and HSE06 methods, as illustrated in Fig. 2. The red dashed circles within the figure display the first Brillouin zone of 2D DJ double-perovskite $(C_6H_{16}N_2)_2AgBiX_8{\cdot}H_2O$ (X = Cl, Br, I) and the path utilized for band structure calculations. The calculations reveal that 2D double-perovskite $(C_6H_{16}N_2)_2AgBiI_8{\cdot}H_2O$, $(C_6H_{16}N_2)_2AgBiBr_8{\cdot}H_2O$, and $(C_6H_{16}N_2)_2AgBiCl_8{\cdot}H_2O$ all possess indirect band gaps. After accounting for the spin-orbit coupling (SOC) effect, the band gap of all three materials is significantly reduced and the band edge shape is altered, highlighting the necessity of considering SOC. In addition, the split bands indicate a pronounced Rashba effect, potentially induced by a significant distortion of the silver and bismuth octahedra [39]. However, irrespective of the method, the band gap increases as the halogen changes from I to Br to Cl. This suggests that halogen substitution can modulate the band gap of $(C_6H_{16}N_2)_2AgBiX_8{\cdot}H_2O$ (X = Cl, Br, I), consistent with the behavior of other types of halogen perovskites [40–43]. Comparing the experimental band gap (i.e., 1.93 eV) [14] of $(C_6H_{16}N_2)_2AgBiI_8{\cdot}H_2O$ with the theoretical band gap, it is evident that the band gap calculated by the PBE method is closely aligned with the experimental value, whereas the band gap calculated by the PBE + SOC method and by the HSE06 method are underestimated and overestimated, respectively. The pure exchange-correlation function (i.e., the PBE) tends to excessively localize the hole, resulting in an overestimation of the electron–hole interaction and, thus, a reduction in the energy gap [44]. For solid-state systems, this typically results in a significant underestimation of the band gap. However, the localized nature of 2D double-perovskite systems, evident from the flat band edge in Fig. 3, makes the PBE function perform better than the commonly employed range-separated hybrid HSE06 function for solids. Therefore, given that the PBE function can more accurately describe the electronic structure and conserve computational resources, we utilized the PBE function results in the subsequent exploration of luminescence properties.

TABLE I. Calculated molecular dissociation energies of 2D DJ double-perovskite $(C_6H_{16}N_2)_2AgBiX_8{\cdot}H_2O$ (X = Cl, Br, I) and 2D RP double-perovskite $(BA)_4BiAgBr_8{\cdot}(C_6H_{16}N_2)_2AgBiX_8$ (X = Cl, Br, I), which refers to the structure of $(C_6H_{16}N_2)_2AgBiX_8{\cdot}H_2O$ (X = Cl, Br, I) after water removal.

	$E_{\text{dissociation}}$ (eV)
$(C_6H_{16}N_2)_2AgBiI_8{\cdot}H_2O$	10.35
$(C_6H_{16}N_2)_2AgBiBr_8{\cdot}H_2O$	11.50
$(C_6H_{16}N_2)_2AgBiCl_8{\cdot}H_2O$	12.15
$(C_6H_{16}N_2)_2AgBiI_8$	9.88
$(C_6H_{16}N_2)_2AgBiBr_8$	10.91
$(C_6H_{16}N_2)_2AgBiCl_8$	11.51
$(BA)_4BiAgBr_8$	5.43

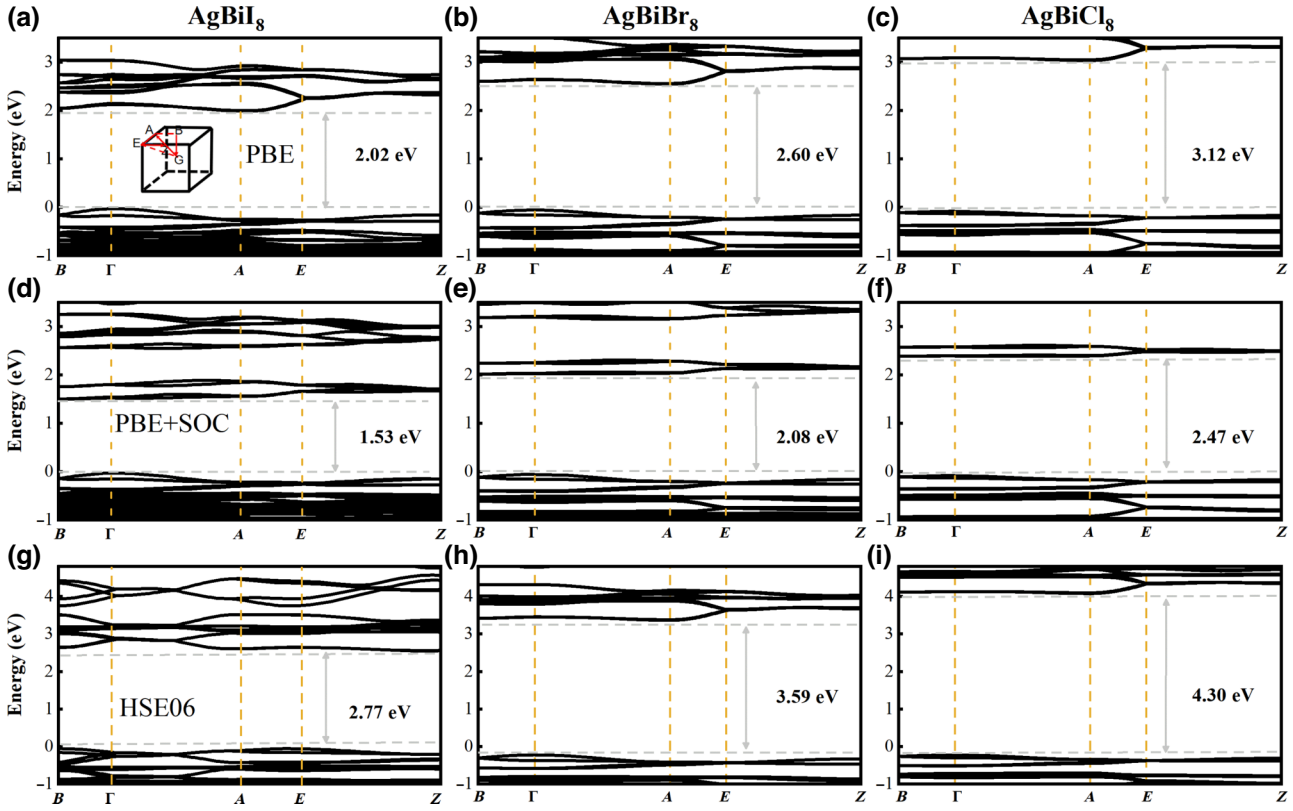

FIG. 2. Band structures of 2D DJ double-perovskite $(C_6H_{16}N_2)_2AgBiX_8{\cdot}H_2O$ (X = Cl, Br, I). Band structures of $(C_6H_{16}N_2)_2AgBiI_8{\cdot}H_2O$ calculated using the (a) PBE, (d) PBE + SOC, and (g) HSE06 methods. Band structures of $(C_6H_{16}N_2)_2AgBiBr_8{\cdot}H_2O$ calculated using the (b) PBE, (e) PBE + SOC, and (h) HSE06 methods. Band structures of $(C_6H_{16}N_2)_2AgBiCl_8{\cdot}H_2O$ calculated using the (c) PBE, (f) PBE + SOC, and (i) HSE06 methods. The inset of (a) shows the first Brillouin zone and the k-path for band structure calculations of 2D DJ double-perovskite $(C_6H_{16}N_2)_2AgBiX_8{\cdot}H_2O$ (X = Cl, Br, I). For simplicity, $(C_6H_{16}N_2)_2AgBiX_8{\cdot}H_2O$ (X = Cl, Br, I) is abbreviated as $AgBiX_8$.

To further explore the regulation of the energy band by halogens, we calculated the partial density of states of $(C_6H_{16}N_2)_2AgBiX_8{\cdot}H_2O$ (X = Cl, Br, I) using the PBE method (Fig. S3 in the Supplemental Material [61]) and the PBE + SOC method (Fig. S2 in the Supplemental Material [61]). Figs. S2 and S3 reveal that the conduction band of 2D DJ double-perovskite $(C_6H_{16}N_2)_2AgBiX_8{\cdot}H_2O$ (X = Cl, Br, I) is primarily composed of Bi-p and X-p (X = Cl, Br, I) orbitals, while the valence band is mainly composed of Ag-d and X-p (X = Cl, Br, I) orbitals. To intuitively observe the effect of halogen on the band gap, we compared the total density of states with the density of projected states, as shown in Fig. S4 within the Supplemental Material [61]. Figure S4(b) in the Supplemental Material [61] illustrates that the energies of I-p, Br-p, and Cl-p orbitals are at the same level in the valence band. Figure S4(c) in the Supplemental Material [61] demonstrates that, in the conduction band, the energy of X-p orbitals increases progressively as X changes from I to Br to Cl, consistent with the change in band gap among $(C_6H_{16}N_2)_2AgBiI_8{\cdot}H_2O$, $(C_6H_{16}N_2)_2AgBiBr_8{\cdot}H_2O$, and $(C_6H_{16}N_2)_2AgBiCl_8{\cdot}H_2O$. Therefore, it can be concluded that the change in the band gap is caused by the change in X-p (X = Cl, Br, I) orbitals. In addition, our calculations indicate that, in all three systems, organic cations make almost no contribution near the Fermi level and merely provide structural support, similar to Cs ions in 2D RP pure inorganic double-perovskite $CsAgBiX_8$ (X = Cl, Br, I). After examining the effects of the halogens on the energy band structure, we now discuss their impact on light absorption properties. The optical absorption coefficient of 2D DJ double-perovskite $(C_6H_{16}N_2)_2AgBiX_8{\cdot}H_2O$ (X = Cl, Br, I), calculated using the PBE and PBE + SOC methods, is presented in Figs. S5 and S6 within the Supplemental Material [61]. The calculations indicate that these three materials exhibit high absorption coefficients in the UV region, with the absorption coefficients decreasing monotonically as the halogen changes from I to Br to Cl.

Table II shows the effective mass and exciton binding energy for 2D DJ double-perovskite $(C_6H_{16}N_2)_2AgBiX_8{\cdot}H_2O$ (X = Cl, Br, I). From the calculations, it is evident that the effective mass and exciton binding energy gradually increase as the halogen changes from I to Br to

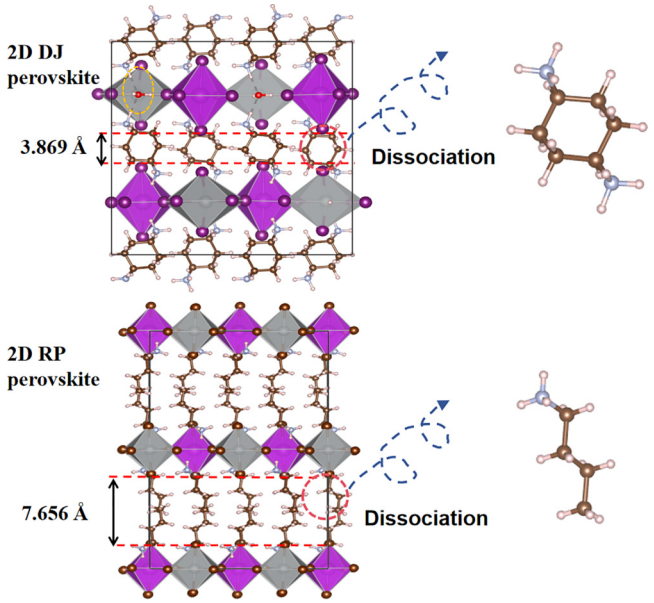

FIG. 3. Schematic illustration of the dissociation of organic groups in 2D DJ double-perovskite $(C_6H_{16}N_2)_2AgBiI_8{\cdot}H_2O$ and 2D RP double-perovskite $(BA)_4AgBiI_8$. The horizontal dashed lines indicate the layer spacing.

Cl. This indicates that halogen substitution can effectively regulate the effective mass and exciton binding energy of 2D DJ double-perovskite materials, thereby modulating their luminescence properties. The exciton binding energy is closely related to the free exciton (FE) emission, and the emission energy of the FE can be calculated using the formula $E_{PL} = E_{gap} - E_b$. The effective mass is associated with self-trapped exciton (STE) emission. Yan and his team [45] have confirmed that low electron dimensionality (i.e., a large effective mass and a flat band) is a key factor in triggering STE. Thus, based on the effective mass results,

TABLE II. Effective mass and exciton binding energy for $(C_6H_{16}N_2)_2AgBiX_8{\cdot}H_2O$ (X = Cl, Br, I) calculated using the PBE + SOC method. Here, E_b denotes the exciton binding energy.

	Conduction band (m_e^*)	Valence band (m_h^*)	E_b (eV)
$(C_6H_{16}N_2)_2AgBiI_8{\cdot}H_2O$	0.51	1.06	0.19
$(C_6H_{16}N_2)_2AgBiBr_8{\cdot}H_2O$	0.81	1.41	0.52
$(C_6H_{16}N_2)_2AgBiCl_8{\cdot}H_2O$	1.21	1.64	0.97

$(C_6H_{16}N_2)_2AgBiBr_8{\cdot}H_2O$ and $(C_6H_{16}N_2)_2AgBiCl_8{\cdot}H_2O$ appear to be more prone to STE.

Due to the tight connectivity of octahedra, three-dimensional perovskites typically exhibit the narrowband emission characteristics of free exciton recombination. In contrast, one- and zero-dimensional perovskites, owing to their relatively isolated inorganic units, generally exhibit the broadband emission characteristics of self-trapped exciton recombination. Compared with three- and one-dimensional (or zero-dimensional) perovskites, the photoluminescence of 2D perovskites is more diverse. Some 2D perovskite materials exhibit free exciton emission, while others show self-trapped exciton emission. To study the luminescence mechanism of 2D DJ double-perovskite $(C_6H_{16}N_2)_2AgBiX_8{\cdot}H_2O$ (X = Cl, Br, I), we calculated its excited-state structure. Based on the computed stable excited-state structure, we plotted the configuration coordinate diagram as shown in Fig. 4. Here, E_{st} represents the energy difference between the free exciton state and the self-trapped state and E_d denotes the lattice deformation energy. According to the Franck-Condon principle, using the formula $E_{PL\text{-}FE} = E_{gap} - E_b$, we calculated the emission energies of self-trapped excitons ($E_{PL\text{-}STE}$) and free excitons ($E_{PL\text{-}FE}$). The specific values of E_{st}, E_d, $E_{PL\text{-}STE}$, and $E_{PL\text{-}FE}$ are shown in Table III. Here, E_{st} reflects the depth of self-trapping; the larger the E_{st} of a material, the more

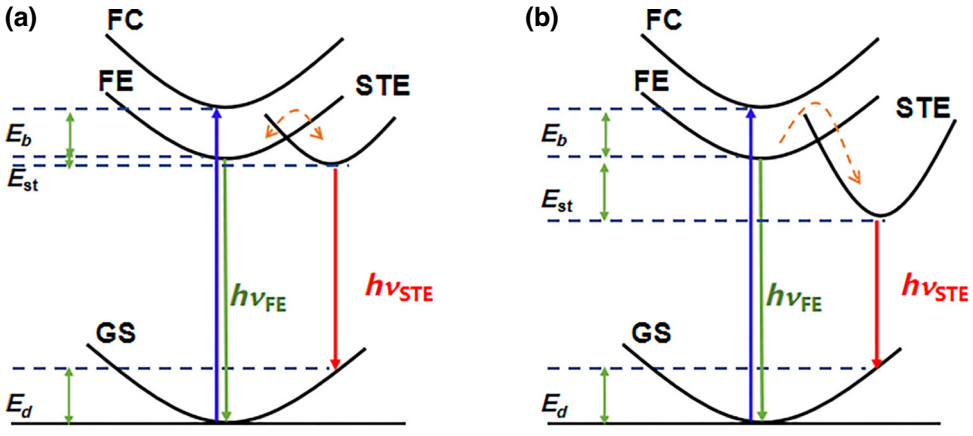

FIG. 4. (a) Configuration coordinate diagram for $(C_6H_{16}N_2)_2AgBiI_8{\cdot}H_2O$. (b) Configuration coordinate diagram for $(C_6H_{16}N_2)_2AgBiBr_8{\cdot}H_2O$ and $(C_6H_{16}N_2)_2AgBiCl_8{\cdot}H_2O$.

TABLE III. Energy differences between states in the configuration coordinate and emission energies of free excitons and self-trapped excitons. Here, E_{st} represents the energy difference between the free excitons excited state and the self-trapped excitons excited state, E_d denotes the lattice deformation energy, which is the energy difference between the self-trapped excitons ground state structure and the ground state structure, and $E_{PL\text{-}STE}$ and $E_{PL\text{-}FE}$ represent the emission energies of self-trapped excitons and free excitons, respectively.

	E_{st} (eV)	E_d (eV)	$E_{PL\text{-}STE}$ (eV)	$E_{PL\text{-}FE}$ (eV)
$(C_6H_{16}N_2)_2AgBiI_8{\cdot}H_2O$	0.08	0.12	1.63	1.83
$(C_6H_{16}N_2)_2AgBiBr_8{\cdot}H_2O$	0.77	0.50	1.46	2.08
$(C_6H_{16}N_2)_2AgBiCl_8{\cdot}H_2O$	0.96	0.58	1.39	2.14

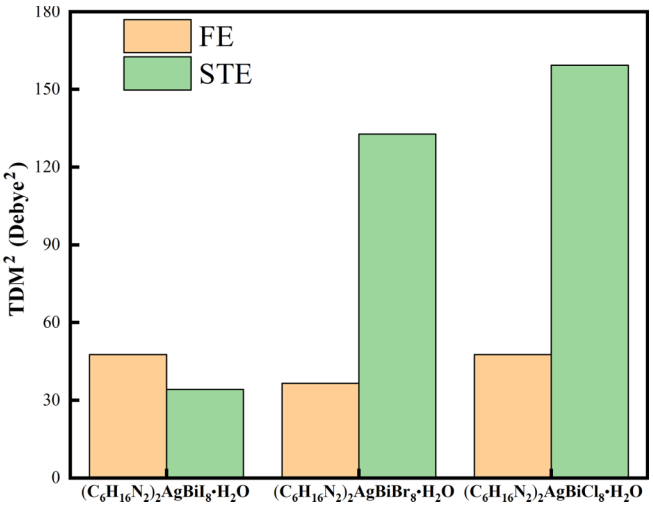

FIG. 5. Transition dipole moments for the free exciton state and self-trapped exciton state of $(C_6H_{16}N_2)_2AgBiX_8{\cdot}H_2O$ (X = Cl, Br, I).

difficult it is for excitons to detrap from the STE state to the FE state.

From the calculations, it is evident that the self-trapping formation energy of $(C_6H_{16}N_2)_2AgBiI_8{\cdot}H_2O$ is very low, and excitons can easily detrap from the STE state to the FE state. Therefore, the STE state may not be stable at room temperature. The experimentally measured emission energy of $(C_6H_{16}N_2)_2AgBiI_8{\cdot}H_2O$ is approximately 1.85 eV, which is consistent with the calculated free exciton emission energy, confirming our hypothesis and the reliability of the calculations [14]. The self-trapping formation energies of $(C_6H_{16}N_2)_2AgBiBr_8{\cdot}H_2O$ and $(C_6H_{16}N_2)_2AgBiCl_8{\cdot}H_2O$ are relatively high, making it difficult for excitons to gain the thermal energy needed to detrap to the free exciton state. Therefore, their STE states are stable. Due to the lower energy of STE, which is thermodynamically more favorable, the luminescence of $(C_6H_{16}N_2)_2AgBiBr_8{\cdot}H_2O$ and $(C_6H_{16}N_2)_2AgBiCl_8{\cdot}H_2O$ will predominantly arise from the STE. The above results indicate that different halogens can result in varying self-trapping depths in 2D DJ double perovskites, thereby affecting their luminescence mechanisms. We speculate that the larger mass and volume of the I atom make the $[PbI_6]^{4-}$ octahedron more resistant to deformation, resulting in less distortion of the $[PbI_6]^{4-}$ octahedron under strong electron-phonon coupling, thereby leading to smaller E_{st} and E_d in iodide perovskites.

The PLQY is defined as the ratio of the radiative recombination rate to the total recombination rate, which includes both nonradiative and radiative recombination rates. According to Fermi's golden rule, the radiative recombination rate is proportional to the transition dipole moment [28]. A qualitative comparison of PLQY using transition dipole moments has been validated and is widely used [12,46–50]. Therefore, by comparing the transition dipole moments, we can qualitatively assess the effects of halogens on the PLQY of $(C_6H_{16}N_2)_2AgBiX_8{\cdot}H_2O$ (X = Cl, Br, I). Figure 5 shows the transition dipole moments of the STE and FE structures for $(C_6H_{16}N_2)_2AgBiX_8{\cdot}H_2O$ (X = Cl, Br, I). First, we find that, for $(C_6H_{16}N_2)_2AgBiI_8{\cdot}H_2O$, the transition dipole moment of the FE structure is slightly larger than that of the STE structure, indicating that $(C_6H_{16}N_2)_2AgBiI_8{\cdot}H_2O$ is more suitable for FE emission. For $(C_6H_{16}N_2)_2AgBiBr_8{\cdot}H_2O$ and $(C_6H_{16}N_2)_2AgBiCl_8{\cdot}H_2O$, the transition dipole moment of the STE structure is greater than that of the FE structure, indicating that $(C_6H_{16}N_2)_2AgBiBr_8{\cdot}H_2O$ and $(C_6H_{16}N_2)_2AgBiCl_8{\cdot}H_2O$ are more suitable for STE emission. In addition, we find that the transition dipole moment of the STE structure of $(C_6H_{16}N_2)_2AgBiBr_8{\cdot}H_2O$ and $(C_6H_{16}N_2)_2AgBiCl_8{\cdot}H_2O$ is significantly higher than that of the FE structure of the three materials. Since $(C_6H_{16}N_2)_2AgBiBr_8{\cdot}H_2O$ and $(C_6H_{16}N_2)_2AgBiCl_8{\cdot}H_2O$ are predominantly STE, they will exhibit stronger luminous efficiency than $(C_6H_{16}N_2)_2AgBiI_8{\cdot}H_2O$. These results suggest that halogens can enhance the luminescence performance of 2D DJ double perovskites by altering their luminescence mechanism. In addition, 2D DJ-chloride double perovskite is expected to exhibit superior luminescence performance compared with 2D DJ-bromide double and DJ-iodide double perovskites.

The transition dipole moment is proportional to the overlap of the electron and hole wave functions; therefore, changes in the transition dipole moment can be elucidated by analyzing the changes in partial charge density. Figures 6 and S10 (within the Supplemental Material [61]) depict the partial charge densities of the FE and STE states for 2D DJ double-perovskite $(C_6H_{16}N_2)_2AgBiI_8{\cdot}H_2O$, $(C_6H_{16}N_2)_2AgBiBr_8{\cdot}H_2O$, and $(C_6H_{16}N_2)_2AgBiCl_8{\cdot}H_2O$. The calculations indicate that the differences in partial charge density between the FE and STE states of $(C_6H_{16}N_2)_2AgBiI_8{\cdot}H_2O$ are minimal. This is because the

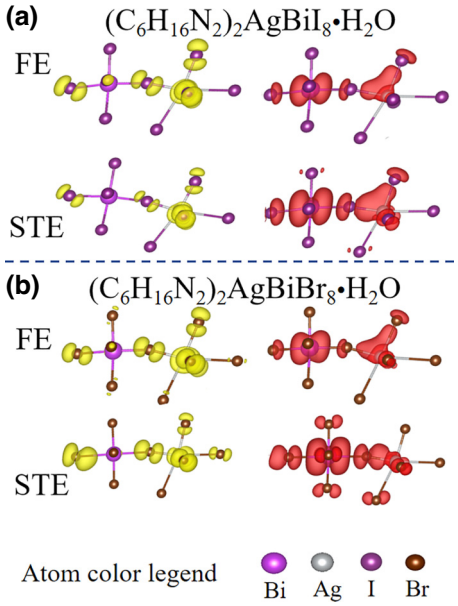

FIG. 6. Partial charge density of $(C_6H_{16}N_2)_2AgBiI_8 \cdot H_2O$ and $(C_6H_{16}N_2)_2AgBiBr_8 \cdot H_2O$. The yellow and red isosurfaces represent the distribution of holes and electrons, respectively. The isosurface value is set at 0.0008 eÅ.

structural differences between the FE and STE states of $(C_6H_{16}N_2)_2AgBiI_8 \cdot H_2O$ are minimal (i.e., a small E_d). For $(C_6H_{16}N_2)_2AgBiBr_8 \cdot H_2O$ and $(C_6H_{16}N_2)_2AgBiCl_8 \cdot H_2O$, the significant structural differences between the FE and STE states (a large E_d) result in noticeable changes in the partial charge density. This difference causes a significant increase in the overlap of electron and hole wave functions at the connection between the Bi octahedron and the Ag octahedron in their STE structures. This also explains why the STE state in $(C_6H_{16}N_2)_2AgBiBr_8 \cdot H_2O$ and $(C_6H_{16}N_2)_2AgBiCl_8 \cdot H_2O$ exhibits a larger transition dipole moment compared with the FE state.

IV. CONCLUSION

In conclusion, this study discusses the effects of halogens on the stability, electronic structure, and luminescence properties of 2D DJ double-perovskite $(C_6H_{16}N_2)_2AgBiX_8 \cdot H_2O$ (X = Cl, Br, I) in detail. In terms of stability, as the halogen changes from I to Br to Cl, the dissociation energy of $(C_6H_{16}N_2)_2AgBiX_8 \cdot H_2O$ (X = Cl, Br, I) gradually increases, indicating that replacing I with a lighter halogen improves the material's stability. Regarding electronic structure, $(C_6H_{16}N_2)_2AgBiX_8 \cdot H_2O$ (X = Cl, Br, I) follows the same trend as other halogen perovskites; as the halogen changes from Cl to Br to I, the band gap gradually decreases while light absorption gradually increases. Concerning luminescence properties, the luminescence mechanism of $(C_6H_{16}N_2)_2AgBiI_8 \cdot H_2O$ is primarily free exciton emission, resulting in relatively low luminescence efficiency. The luminescence of $(C_6H_{16}N_2)_2AgBiBr_8 \cdot H_2O$ and $(C_6H_{16}N_2)_2AgBiCl_8 \cdot H_2O$ is primarily STE, with higher luminous efficiency. In summary, our study successfully regulated the stability and luminescence properties of 2D DJ double perovskites using halogens. These results provide theoretical guidance for designing superior luminescent materials.

The data that support the findings of this study are available from the corresponding authors upon reasonable request.

ACKNOWLEDGMENT

The authors thank Ms. Lee Juan for her support. This work is supported by the National Natural Science Foundation of China (Grant No. 51972103) and the National Natural Science Foundation of Guangdong (Grant No. 2024A151501396).

There are no conflicts of interest to declare.

[1] Y. Shang, Y. Liao, Q. Wei, Z. Wang, B. Xiang, Y. Ke, W. Liu, and Z. Ning, Highly stable hybrid perovskite light-emitting diodes based on Dion-Jacobson structure, Sci. Adv. **5**, eaaw8072 (2019).

[2] C. Zhou, H. Lin, Q. He, L. Xu, M. Worku, M. Chaaban, S. Lee, X. Shi, M.-H. Du, and B. Ma, Low dimensional metal halide perovskites and hybrids, Mater. Sci. Eng., R **137**, 38 (2019).

[3] Y. Jiang, M. Cui, S. Li, C. Sun, Y. Huang, J. Wei, L. Zhang, M. Lv, C. Qin, Y. Liu, *et al.*, Reducing the impact of Auger recombination in quasi-2D perovskite light-emitting diodes, Nat. Commun. **12**, 336 (2021).

[4] C. Pareja-Rivera, J. A. Morán-Muñoz, A. P. Gómora-Figueroa, V. Jancik, B. Vargas, J. Rodríguez-Hernández, and D. Solis-Ibarra, Optimizing broadband emission in 2D halide perovskites, Chem. Mater. **34**, 9344 (2022).

[5] S. Sun, M. Lu, X. Gao, Z. Shi, X. Bai, W. W. Yu, and Y. Zhang, 0D perovskites: Unique properties, synthesis, and their applications, Adv. Sci. (Weinh) **8**, e2102689 (2021).

[6] Y. Liu, L. K. Ono, G. Tong, H. Zhang, and Y. Qi, Two-dimensional Dion–Jacobson structure perovskites for efficient sky-blue light-emitting diodes, ACS Energy Lett. **6**, 908 (2021).

[7] C. C. Stoumpos, D. H. Cao, D. J. Clark, J. Young, J. M. Rondinelli, J. I. Jang, J. T. Hupp, and M. G. Kanatzidis, Ruddlesden–Popper hybrid lead iodide perovskite 2D homologous semiconductors, Chem. Mater. **28**, 2852 (2016).

[8] L. Mao, W. Ke, L. Pedesseau, Y. Wu, C. Katan, J. Even, M. R. Wasielewski, C. C. Stoumpos, and M. G. Kanatzidis, Hybrid Dion-Jacobson 2D lead iodide perovskites, J. Am. Chem. Soc. **140**, 3775 (2018).

[9] L. Li, H. Shao, X. Wu, W. Chen, J. Zhu, B. Dong, L. Xu, W. Xu, J. Hu, M. Zhou, *et al.*, Aluminum-doped lead-free double perovskite $Cs_2AgBiCl_6$ nanocrystals with ultrahigh

stability towards white light emitting diodes, Mater. Res. Bull. **147**, 111645 (2022).

[10] M.-W. Zeng, Y.-Q. Zhao, and M.-Q. Cai, Effects of halogen substitution on the optoelectronic properties of two-dimensional all-inorganic double perovskite Cs_4AgBiX_8 (X = Cl, Br, I) with Ruddlesden-Popper structure, Phys. Rev. Appl. **16**, 054019 (2021).

[11] Z. Liu, Y. Sun, T. Cai, H. Yang, J. Zhao, T. Yin, C. Hao, M. Chen, W. Shi, X. Li, *et al.*, Two-dimensional $Cs_2AgIn_xBi_{1-x}Cl_6$ alloyed double perovskite nanoplatelets for solution-processed light-emitting diodes, Adv. Mater. **35**, e2211235 (2023).

[12] J. Luo, X. Wang, S. Li, J. Liu, Y. Guo, G. Niu, L. Yao, Y. Fu, L. Gao, Q. Dong, *et al.*, Efficient and stable emission of warm-white light from lead-free halide double perovskites, Nature **563**, 541 (2018).

[13] F. Locardi, M. Cirignano, D. Baranov, Z. Dang, M. Prato, F. Drago, M. Ferretti, V. Pinchetti, M. Fanciulli, S. Brovelli, *et al.*, Colloidal synthesis of double perovskite $Cs_2AgInCl_6$ and Mn-doped $Cs_2AgInCl_6$ nanocrystals, J. Am. Chem. Soc. **140**, 12989 (2018).

[14] L.-Y. Bi, Y.-Q. Hu, M.-Q. Li, T.-L. Hu, H.-L. Zhang, X.-T. Yin, W.-X. Que, M. S. Lassoued, and Y.-Z. Zheng, Two-dimensional lead-free iodide-based hybrid double perovskites: crystal growth, thin-film preparation and photocurrent responses, J. Mater. Chem. A **7**, 19662 (2019).

[15] Y. L. Chen, D. N. Yan, M. W. Zeng, C. S. Liao, and M. Q. Cai, 2D and 3D double perovskite with dimensionality-dependent optoelectronic properties: First-principle study on $Cs_2AgBiBr_6$ and $Cs_4AgBiBr_8$, J. Phys.: Condens. Matter **34**, 065501 (2022).

[16] G. Kresse and D. Joubert, From ultrasoft pseudopotentials to the projector augmented-wave method, Phys. Rev. B **59**, 1758 (1999).

[17] D.-N. Yan, C.-S. Liao, Y.-Q. Zhao, B. Liu, J.-L. Yang, and M.-Q. Cai, Theoretical prediction of double perovskite $Cs_2Ag_xCu_{1-x}In_yTb_{1-y}Cl_6$ for infrared detection, J. Phys. D: Appl. Phys. **53**, 265302 (2020).

[18] Y.-Q. Zhao, Z.-S. Liu, G.-Z. Nie, Z.-H. Zhu, Y.-F. Chai, J.-N. Wang, M.-Q. Cai, and S. Jiang, Structural, electronic, and charge transfer features for two kinds of MoS_2/Cs_2PbI_4 interfaces with optoelectronic applicability: Insights from first-principles, Appl. Phys. Lett. **118**, 173104 (2021).

[19] C.-J. Zhong, J. Luo, L.-Y. Pan, B. Liu, J. Yang, and M.-Q. Cai, Theoretical study on photoelectric properties of ferroelectric photovoltaic perovskite $CsGeBr_3$ based on first-principle calculations, Phys. Scr. **99**, 065982 (2024).

[20] L.-l. Zhang, J. Luo, B. Liu, J. Yang, and M.-Q. Cai, Effect of substituting on the transition dipole moment of the double perovskite $Cs_2AgInCl_6$, J. Phys.: Condens. Matter **36**, 075703 (2024).

[21] G. Giorgi, K. Yamashita, and M. Palummo, Nature of the electronic and optical excitations of ruddlesden-popper hybrid organic-inorganic perovskites: The role of the many-body interactions, J. Phys. Chem. Lett. **9**, 5891 (2018).

[22] B. Liu, X. Feng, M. Long, M.-Q. Cai, and J. Yang, Designing surface-functionalized $Ti_3C_2T_2-Cs_3Bi_2Br_9$(T = O, Cl, OH, or F) heterostructures for perovskite optoelectronic applications, Phys. Rev. Appl. **18**, 054036 (2022).

[23] X. Feng, Y. Li, M. Long, M. Cai, B. Liu, and J. Yang, The key role of methylenediammonium and tetrahydrotriazinium in the phase stability of $FAPbI_3$, Appl. Phys. Lett. **124**, 193903 (2024).

[24] D. L. Busipalli, K. Y. Lin, S. Nachimuthu, and J. C. Jiang, Enhanced moisture stability of cesium lead iodide perovskite solar cells – A first-principles molecular dynamics study, Phys. Chem. Chem. Phys. **22**, 5693 (2020).

[25] X. Z. Deng, J. R. Zhang, Y. Q. Zhao, Z. L. Yu, J. L. Yang, and M. Q. Cai, The energy band engineering for the high-performance infrared photodetectors constructed by $CdTe/MoS_2$ heterojunction, J. Phys.: Condens. Matter. **32**, 065004 (2020).

[26] U.-G. Jong, C.-J. Yu, J.-S. Ri, N.-H. Kim, and G.-C. Ri, Influence of halide composition on the structural, electronic, and optical properties of mixed $CH_3NH_3Pb(I_{1-x}Br_x)_3$ perovskites calculated using the virtual crystal approximation method, Phys. Rev. B **94**, 125139 (2016).

[27] S. Baroni and R. Resta, Ab initio calculation of the macroscopic dielectric constant in silicon, Phys. Rev. B **33**, 7017 (1986).

[28] J. Luo, B. Liu, J.-L. Yang, and M.-Q. Cai, Regulation of luminescence properties of the ultrathin two-dimensional halide perovskite $Cs_2PbI_xCl_{4-x}$ (x = 0,1,2,3,4) with Ruddlesden-Popper structure, Phys. Rev. Appl. **20**, 024047 (2023).

[29] B. A. Connor, L. Leppert, M. D. Smith, J. B. Neaton, and H. I. Karunadasa, Layered halide double perovskites: Dimensional reduction of $Cs_2AgBiBr_6$, J. Am. Chem. Soc. **140**, 5235 (2018).

[30] C. Eames, J. M. Frost, P. R. F. Barnes, B. C. O'Regan, A. Walsh, and M. S. Islam, Ionic transport in hybrid lead iodide perovskite solar cells, Nat. Commun. **6**, 7497 (2015).

[31] E. T. Hoke, D. J. Slotcavage, E. R. Dohner, A. R. Bowring, H. I. Karunadasa, and M. D. McGehee, Reversible photo-induced trap formation in mixed-halide hybrid perovskites for photovoltaics, Chem. Sci. **6**, 613 (2015).

[32] Z. Li, C. Xiao, Y. Yang, S. P. Harvey, D. H. Kim, J. A. Christians, M. Yang, P. Schulz, S. U. Nanayakkara, C.-S. Jiang, *et al.*, Extrinsic ion migration in perovskite solar cells, Energy Environ. Sci. **10**, 1234 (2017).

[33] Y. Tian, C. Zhou, M. Worku, X. Wang, Y. Ling, H. Gao, Y. Zhou, Y. Miao, J. Guan, and B. Ma, Highly efficient spectrally stable red perovskite light-emitting diodes, Adv. Mater. **30**, 1707093 (2018).

[34] J. Peng, C. Q. Xia, Y. Xu, R. Li, L. Cui, J. K. Clegg, L. M. Herz, M. B. Johnston, and Q. Lin, Crystallization of $CsPbBr_3$ single crystals in water for X-ray detection, Nat. Commun. **12**, 1531 (2021).

[35] Z. Liu, L. Qiu, L. K. Ono, S. He, Z. Hu, M. Jiang, G. Tong, Z. Wu, Y. Jiang, D.-Y. Son, *et al.*, A holistic approach to interface stabilization for efficient perovskite solar modules with over 2,000-hour operational stability, Nat. Energy **5**, 596 (2020).

[36] X. Zhang, X. Bai, H. Wu, X. Zhang, C. Sun, Y. Zhang, W. Zhang, W. Zheng, W. W. Yu, and A. L. Rogach, Water-assisted size and shape control of CsPbBr(3) perovskite nanocrystals, Angew. Chem., Int. Ed. Engl. **57**, 3337 (2018).

[37] L. Ling, S. Yuan, P. Wang, H. Zhang, L. Tu, J. Wang, Y. Zhan, and L. Zheng, Precisely controlled hydration water for performance improvement of organic–inorganic perovskite solar cells, Adv. Funct. Mater. **26**, 5028 (2016).

[38] J. W. Lee, D. H. Kim, H. S. Kim, S. W. Seo, S. M. Cho, and N. G. Park, Formamidinium and cesium hybridization for photo- and moisture-stable perovskite solar cell, Adv. Energy Mater. **5**, 1501310 (2015).

[39] J. Yin, P. Maity, L. Xu, A. M. El-Zohry, H. Li, O. M. Bakr, J.-L. Brédas, and O. F. Mohammed, Layer-dependent Rashba band splitting in 2D hybrid perovskites, Chem. Mater. **30**, 8538 (2018).

[40] Y. J. Cao, L. Zhou, L. He, P. P. Shi, Q. Ye, and D. W. Fu, Phase transition and band gap regulation by halogen substituents on the organic cation in organic-inorganic hybrid perovskite semiconductors, Chemistry **26**, 14124 (2020).

[41] H. Liu, X. Li, Y. Zeng, and L. Meng, Effects of halogen substitutions on the properties of $CH_3NH_3Sn_{0.5}Pb_{0.5}I_3$ perovskites, Comput. Mater. Sci. **177**, 109576 (2020).

[42] C. Chen, Y. Kuai, X. Li, J. Hao, L. Li, Y. Liu, X. Ma, L. Wu, and P. Lu, Impact of halogen substitution on the electronic and optical properties of 2D lead-free hybrid perovskites, J. Phys. Chem. C **125**, 15742 (2021).

[43] M.-M. Zhao, L. Zhou, P.-P. Shi, X. Zheng, X.-G. Chen, J.-X. Gao, F.-J. Geng, Q. Ye, and D.-W. Fu, Halogen substitution effects on optical and electrical properties in 3D molecular perovskites, Chem. Commun. **54**, 13275 (2018).

[44] R. van Meer, O. V. Gritsenko, and E. J. Baerends, Physical meaning of virtual Kohn-Sham orbitals and orbital energies: An ideal basis for the description of molecular excitations, J. Chem. Theory Comput. **10**, 4432 (2014).

[45] X. Wang, W. Meng, W. Liao, J. Wang, R. G. Xiong, and Y. Yan, Atomistic mechanism of broadband emission in metal halide perovskites, J. Phys. Chem. Lett. **10**, 501 (2019).

[46] L. L. Zhang, J. Luo, B. Liu, J. Yang, and M. Q. Cai, Effect of substituting on the transition dipole moment of the double perovskite $Cs_2AgInCl_6$, J. Phys.: Condens. Matter. **36**, 075703 (2024).

[47] M. J. Jurow, T. Morgenstern, C. Eisler, J. Kang, E. Penzo, M. Do, M. Engelmayer, W. T. Osowiecki, Y. Bekenstein, C. Tassone, *et al.*, Manipulating the transition dipole moment of $CsPbBr_3$ perovskite nanocrystals for superior optical properties, Nano Lett. **19**, 2489 (2019).

[48] C. Xue, H. Huang, S. Nishihara, V. Biju, X. M. Ren, and T. Nakamura, Inorganic chain mediated excitonic properties in one-dimensional lead halide hybrid perovskites, J. Phys. Chem. Lett. **13**, 7405 (2022).

[49] Y. Wang, Q. Song, W. Hu, D. Wang, L. Peng, T. Shi, X. Liu, Y. Zhu, and J. Lin, Temperature-driven phase transition and transition dipole moment of two-dimensional $BA_2CsPb_2Br_7$ perovskite, Phys. Chem. Chem. Phys. **23**, 16341 (2021).

[50] W. Meng, B. Saparov, F. Hong, J. Wang, D. B. Mitzi, and Y. Yan, Alloying and defect control within chalcogenide perovskites for optimized photovoltaic application, Chem. Mater. **28**, 821 (2016).

[51] E. R. Dohner, A. Jaffe, L. R. Bradshaw, and H. I. Karunadasa, Intrinsic white-light emission from layered hybrid perovskites, J. Am. Chem. Soc. **136**, 13154 (2014).

[52] E. R. Dohner, E. T. Hoke, and H. I. Karunadasa, Self-assembly of broadband white-light emitters, J. Am. Chem. Soc. **136**, 1718 (2014).

[53] A. Yangui, D. Garrot, J. S. Lauret, A. Lusson, G. Bouchez, E. Deleporte, S. Pillet, E. E. Bendeif, M. Castro, S. Triki, *et al.*, Optical investigation of broadband white-light emission in self-assembled organic–inorganic perovskite $(C_6H_{11}NH_3)_2PbBr_4$, J. Phys. Chem. C **119**, 23638 (2015).

[54] Y. Y. Li, C. K. Lin, G. L. Zheng, Z. Y. Cheng, H. You, W. D. Wang, and J. Lin, Novel <110>-oriented organic−inorganic perovskite compound stabilized by *N*-(3-Aminopropyl)imidazole with improved optical properties, Chem. Mater. **18**, 3463 (2006).

[55] K. Thirumal, W. K. Chong, W. Xie, R. Ganguly, S. K. Muduli, M. Sherburne, M. Asta, S. Mhaisalkar, T. C. Sum, H. S. Soo, *et al.*, Morphology-independent stable white-light emission from self-assembled two-dimensional perovskites driven by strong exciton–phonon coupling to the organic framework, Chem. Mater. **29**, 3947 (2017).

[56] L. Mao, Y. Wu, C. C. Stoumpos, B. Traore, C. Katan, J. Even, M. R. Wasielewski, and M. G. Kanatzidis, Tunable white-light emission in single-cation-templated three-layered 2D perovskites $(CH_3CH_2NH_3)_4Pb_3Br_{10-x}Cl_x$, J. Am. Chem. Soc. **139**, 11956 (2017).

[57] K.-z. Du, Q. Tu, X. Zhang, Q. Han, J. Liu, S. Zauscher, and D. B. Mitzi, Two-dimensional lead(II) halide-based hybrid perovskites templated by acene alkylamines: Crystal structures, optical properties, and piezoelectricity, Inorg. Chem. **56**, 9291 (2017).

[58] D. Cortecchia, S. Neutzner, A. R. Srimath Kandada, E. Mosconi, D. Meggiolaro, F. De Angelis, C. Soci, and A. Petrozza, Broadband emission in two-dimensional hybrid perovskites: The role of structural deformation, J. Am. Chem. Soc. **139**, 39 (2017).

[59] X. Huang, Y. Wang, Y. Weng, Z. Yang, and S. Dong, Stability, electronic, and optical properties of lead-free halide double perovskites $(CH_3NH_3)_2InBiX_6$ (X = halogen), Phys. Rev. Mater. **4**, 104601 (2020).

[60] D. L. Busipalli, K.-Y. Lin, S. Nachimuthu, and J.-C. Jiang, Enhanced moisture stability of cesium lead iodide perovskite solar cells – a first-principles molecular dynamics study, Phys. Chem. Chem. Phys. **22**, 5693 (2020).

[61] See Supplemental Material at http://link.aps.org/supplemental/10.1103/PhysRevApplied.22.014064 for additional details, including thermal stability, band structures, state densities, partial charge density, luminescence analysis, and reference [51–60].